Complex $Ga^0(4p^1)$ and $In^0(5p^1)$ centers in KCl.
Electron-spin-resonance study

Willy Van Puymbroeck

Physics Department, University of Antwerp (U.I.A), B-2610 Wilrijk, Belgium

Johannes Andriessen

Physics Department, University of Technology, 2600 GA Delft, The Netherlands

Dirk Schoemaker

Physics Department, University of Antwerp (U.I.A.), B-2610 Wilrijk, Belgium

A detailed electron-spin-resonance (ESR) study has been made of trapped electron centers in KCl doped with the ns^2 metal ions $M^+ = Ga^+, In^+$. X-ray irradiation at 77 K produces by simple electron trapping the primary M^0 atom defects which manifest themselves as linear symmetric $\langle 100 \rangle$-oriented MCl_2^{2-} molecule ions. Both centers exhibit a reorientation motion with very low activation energy, and the relevance of this for the nonobservability of the primary Tl^0 ESR spectrum is discussed. An x-ray irradiation above 220 K, where negative ion vacancies become mobile, leads to several complex M^0 defects. Two of them, called $M^0(1)$ and $M^0(2)$, are analogous to the $Tl^0(1)$ and $Tl^0(2)$ defects studied earlier, and their structures are confirmed: In $M^0(1)$ a M^0 on a cation site is associated with a single anion vacancy, and in $M^0(2)$ the M^0 is flanked by two anion vacancies. For both centers there is an appreciable delocalization of the unpaired electron. An additional center, called Ga^0 (axial), is shown to be in essence an orthorhombic center which exhibits even at ~ 10 K a rapid reorientation between two equivalent Jahn-Teller distortions in a $\{100\}$ plane. An analysis of the ESR parameters reveals regularities in the variation of the isotropic part of the M^0 hyperfine interaction which can be related to the even or odd character of the perturbing crystal field. Extensive data on the production and thermal properties of the different defects are also given.

I. INTRODUCTION

Recently, the structure of several complex trapped electron defects produced by x-ray irradiation in alkali halides doped with ns^2 ($n = 4, 5, 6$) heavy metal impurities have been extensively studied with electron-spin-resonance (ESR). These investigations include the $Sn^+(5p^1)$ (Refs. 1 and 2) and $Sn^-(5p^3)$ (Ref. 3) defects both in KCl:Sn²⁺, Pb⁺(6p¹) in KCl:Pb²⁺ (Refs. 4 and 5) and most recently two $Tl^0(6p^1)$ centers produced in KCl:Tl⁺.[6] Besides purely spectroscopic data these studies have already yielded a great deal of information about the structure of these complex defects and about the mobility of positive and negative ion vacancies and their interaction with the heavy metal ions before and after electron trapping.

From the detailed experimental and theoretical study[6] on two complex Tl^0 defects produced in KCl:Tl⁺ by x-ray irradiation above 230 K it was possible to deduce the precise defect structures: the Tl^0 on a cation site is in the one defect associated with a single anion vacancy and in the other it is flanked by two anion vacancies. However, in agreement with many earlier attempts,[1,4] this study did not yield the ESR spectrum of the primary Tl^0 defect, i.e., a Tl^0 occupying an unperturbed cation vacancy. The primary

Tl^0 defect, formed by simple electron trapping of a substitutional $Tl^+(6s^2)$ impurity, has been identified and thoroughly studied by optical techniques.[7-9]

The present paper contains an extensive ESR study of complex defects produced by x-ray irradiation of KCl doped with $Ga^+(4s^2)$ and $In^+(5s^2)$.[10] This study was undertaken with a threefold aim; first, to see whether or not complex Ga^0 and In^0 defects are produced similar to the Tl^0 ones observed in KCl:Tl⁺ (Ref. 6); second, whether the primary Ga^0 and In^0 centers can be observed in ESR; and third, whether the metal atom in its ground state is on a substitutional lattice site or not. Recent optically detected ESR studies of the relaxed excited $4s4p$ states of the $Ga^+(4s^2)$ ion in alkali halides indicate an off-center position of the impurity ion at least in the excited state.[11]

The structure of the present paper is as follows. It will be shown in Sec. III B that the primary Ga^0 and In^0 centers are indeed observed in ESR and that they manifest themselves as $\langle 100 \rangle$ oriented $GaCl_2^{2-}$ and $InCl_2^{2-}$ species, very similar to the primary $SnCl_2^-$ center in KCl:Sn²⁺.[1] Both defects will be shown to possess a bond-switching reorientation motion between $\langle 100 \rangle$ directions at low temperatures. In Secs. III C and III D two Ga^0 and two In^0 defects will

be discussed which are in all aspects identical to the two Tl^0 defects in KCl:Tl$^+$.[6] These results nicely confirm and strengthen the conclusions made in Ref. 6. Section III D contains also results on a fourth Ga^0 and a fourth In^0 defect called Ga^0 (axial) and In^0 (ortho). It will be argued that for Ga^0 (axial) a fast reorientation motion occurs between two equivalent Jahn-Teller distortions in a {100} plane. The g and hyperfine (hf) data of the different Ga^0 and In^0 centers will be discussed within a simple crystal-field picture in Sec. III E. An unrestricted relativistic Hartree-Fock calculation of these parameters will be presented in a forthcoming paper. All Ga^0 and In^0 models will be extensively discussed in Sec. IV. Production curves and thermal data for the different defects will be presented in Sec. V. Section VI summarizes the most important results obtained in this paper and the nonobservability of the ESR spectrum of the primary Tl^0 is discussed.

II. EXPERIMENTAL

The Ga$^+$- and In$^+$-doped KCl crystals used in these experiments were grown in an HCl atmosphere by the Bridgman method. The Ga$^+$ and In$^+$ concentration varied between 50 and 150 ppm as measured by flame-emission spectrophotometry. It is possible that valence states other than the monovalent one are present in the crystals.

Defects were produced at temperatures between 77 K and room temperature (RT) by short x-ray irradiation (typically about 15 min) using a Siemens tube operating at 50 kV and 50 mA. Before every irradiation the samples were routinely warmed up to about 400 °C for several minutes and then rapidly cooled down to RT. The samples were always handled in the dark. Experimental details on the X-band ESR instrumentation can be found in Refs. 3 and 6.

III. PRODUCTION, DESCRIPTION, AND ANALYSIS OF THE ESR SPECTRA

A. General remarks on the ESR analysis of Ga^0($4p^1$) and In^0($5p^1$) defects

Of the ESR spectra that will be discussed the main feature results from the hf interaction of the unpaired electron with the Ga^0 or In^0 nucleus. Natural Ga has two isotopes, ^{69}Ga and ^{71}Ga, respectively, 60.2% and 39.8% abundant, both with nuclear spin $\frac{3}{2}$ but with distinctly differing nuclear moments: +2.0108 nuclear magnetons (μ_N) and +2.5549μ_N, respectively. The quadrupole moment is small for both Ga isotopes: $+0.178 \times 10^{-24}$ and $+0.112 \times 10^{-24}$ cm^2. The hf pattern resulting from the interaction with the Ga nuclei is composed out of two spectra of four nearly equidistant hf lines. The intensity ratio between the two four-line spectra is 3:2.

The least intense ESR lines have the largest hf separation. The ^{115}In isotope is 95.8% abundant, has nuclear spin $\frac{9}{2}$, a large nuclear magnetic moment ($+5.5073\mu_N$), and a sizable quadrupole moment ($+0.761 \times 10^{-24}$ cm^2). A 10-line ESR pattern results from the hf interaction with the In nuclei. All lines have equal intensity but the spacing between the lines varies noticeably because of higher order hf and quadrupole effects.

The ESR spectra of the various Ga^0 and In^0 centers are fitted to following spin Hamiltonian (in the usual notation):

$$\frac{\mathcal{K}}{g_0\mu_B} = \frac{1}{g_0}\vec{H}\cdot\vec{g}\cdot\vec{S} + \vec{S}\cdot\vec{A}\cdot\vec{I} + PI_z^2 , \qquad (1)$$

with $S = \frac{1}{2}$ and $I = \frac{3}{2}$ or $\frac{9}{2}$ for the Ga or the In nucleus, respectively. The quadrupole interaction, represented by the last term, is not measurable for the Ga^0 defects because of its smallness, but the g and hf parameters are readily obtained by fitting the ESR spectra to a second-order perturbation solution of (1). Indeed, the total hf interaction is much smaller than the Zeeman term. The resulting hf constants quoted in Tables I—IV correspond to the ^{71}Ga isotope. As a check on the ESR parameters the ratio of the ^{71}Ga to the ^{69}Ga hf constants was calculated for all Ga^0 defects. This ratio was found to be equal to $\mu_N(^{71}\text{Ga})/\mu_N(^{69}\text{Ga}) = 1.27$ within experimental accuracy. The situation for the In^0 defects is different. The hf parameter itself and the nuclear spin are so large that the total hf interaction is of the same magnitude as the Zeeman term. The g, hf, and quadrupole data of the In^0 centers as given in Tables I—IV result from a computer diagonalization of (1) employing a suitable fitting procedure. The ESR line positions calculated with these parameters agree very well, i.e., within 0.4 mT, with the experimental ones. The absolute signs of the hf and quadrupole constants cannot be determined from the ESR analysis as such.

Throughout the present paper it is accepted that one is dealing with atom defects and that only one gallium or indium nucleus is involved in the defect structure. The latter is proven by the observed specific hf pattern which originates from a single nucleus. The former can be justified by a reasoning analogous to the one adopted in Ref. 6 where the atomic character of the two Tl^0 centers was established. Furthermore, in Sec. III E a good description of the ESR parameters of the different Ga^0 and In^0 defects is given in terms of a single p electron substantiating the atomic character.

B. Primary Ga^0 and In^0 defects: GaCl$_2^{2-}$ and InCl$_2^{2-}$

The primary Ga^0 and In^0 centers are readily produced by a short (about 10 min) x-ray irradiation of the appropriately doped KCl at 77 K. Figure 1
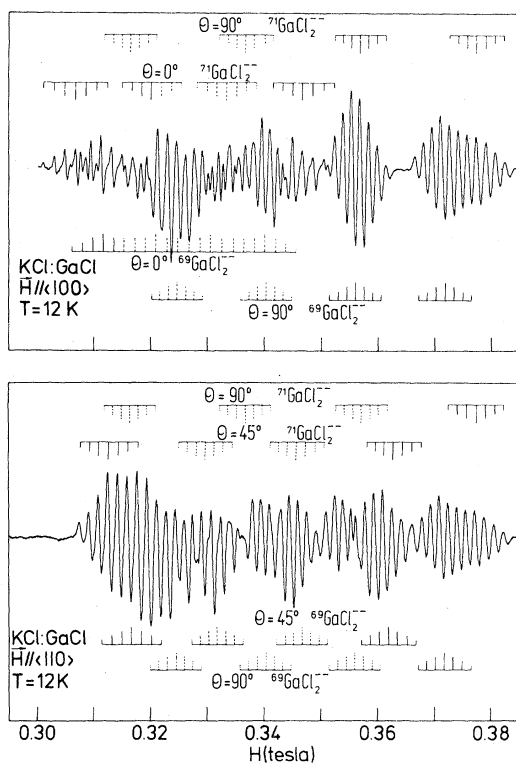
FIG. 1. ESR spectra at $T = 12$ K of the primary $GaCl_2^{2-}$ in KCl:GaCl produced by x-ray irradiation at 77 K. The first derivative of the absorption is presented for two special directions of the magnetic field $\vec{H}$. Here as in Figs. 2 to 7 the microwave frequency $\nu = 9.16$ GHz.

presents the ESR spectra of the primary Ga^0 center. The lines are indicated by the angle θ between the static magnetic field $\vec{H}$ and the symmetry axis, $z \parallel \langle 100 \rangle$, of the defect. The ESR spectra which are found to possess axial symmetry were recorded at 12 K which is the temperature where they are best observable. A characteristic seven-line superhyperfine (shf) structure with intensity ratios 1:2:3:4:3:2:1 is superimposed on the two four-line hf patterns originating from the hf interaction with the two Ga^0 isotope nuclei. The shf structure originates from two equivalent Cl nuclei with no resolved isotope effects. Chlorine has two isotopes ^{35}Cl (75.4% abundant) and ^{37}Cl (24.6% abundant) both with nuclear spin $\frac{3}{2}$.

The seven-line shf structure persists for every value of θ and it is concluded that the primary Ga^0 center consists of a linear symmetric $\langle 100 \rangle$ oriented $(Cl^-Ga^0Cl^-)$ molecule ion. The linewidth ΔH exhibits a small anisotropy and is temperature independent below 25 K. Above 25 K a rapid broadening occurs. At 35 K the chlorine shf structure is no longer resolved. The intensity of the ESR lines decreases rapidly and the line positions move inwards if the

temperaturte is increased above 35 K. These observations point to a thermally activated internal motion of the primary Ga^0 center, very likely a bond switching motion among the three $\langle 100 \rangle$ directions.[1] We did not observe a motional averaged ESR spectrum, which should correspond to a $GaCl_6^{6-}$ structure, possibly because the spin-lattice relaxation time becomes too short at higher temperatures.

The ESR spectra of the primary In^0 center recorded at 10 K are given in Fig. 2. The seven-line shf pattern originating from the interaction with two equivalent Cl nuclei, superimposed on the 10-line In^0 hf structure, is readily recognized for every direction of $\vec{H}$. The lines broaden rapidly above 10 K and the shf structure becomes unresolved when the observation temperature is increased above 18 K, strongly suggesting an internal motion similar to the $GaCl_2^{2-}$ one. The primary In^0 ESR spectrum is best observable at temperatures lower than the one for the primary Ga^0, which suggests a stronger spin-lattice coupling for the former, possibly induced by the rapid reorientation motion.

It should be stressed that the primary $GaCl_2^{2-}$ and primary $InCl_2^{2-}$ center are analogous to the primary Tl^0 defect [designated as[12] $Tl^0(0)$ in Ref. 6] which, in spite of extensive searches, has not yet been observed in ESR at X-band frequencies. This is further discussed in Sec. VI. A similar behavior is observed
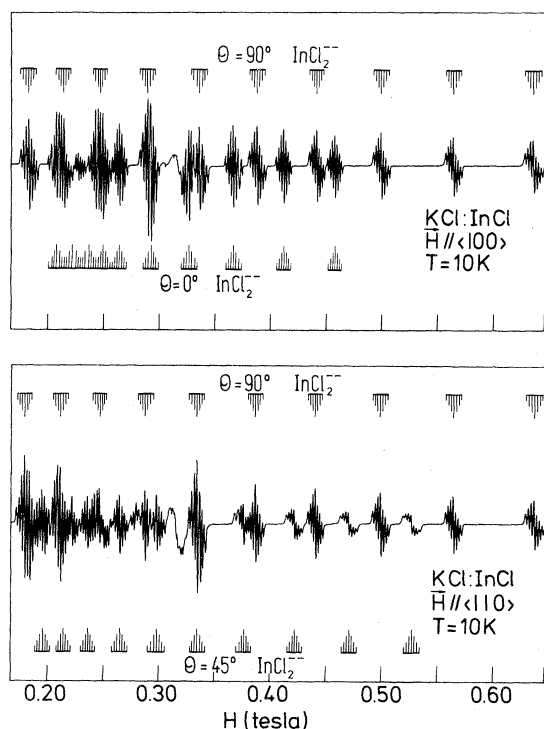

FIG. 2. ESR spectra at $T = 10$ K of the primary $InCl_2^{2-}$ in KCl:InCl produced by x-ray irradiation at 77 K.

TABLE I. The spin-Hamiltonian parameters of the primary $^{71}GaCl_2^{2-}$ in KCl:Ga$^+$ at $T = 15$ K and of the primary $^{115}InCl_2^{2-}$ in KCl:In$^+$ at $T = 12$ K. The ESR parameters of $^{119}SnCl_2^-$(tetrag) in KCl:SnCl$_2$ at 24 K are included for comparison. The hyperfine, superhyperfine, and quadrupole parameters and the linewidth ΔH are given in mT.

Center MCl_2^{2-}	$g_{\parallel}$ [001]	$g_{\perp}$	$A_{\parallel}(M)$[a] [001]	$A_{\perp}(M)$[a]	$a_{\parallel}(Cl)$[a] [001]	$a_{\perp}(Cl)$[a]	$P(M)$	ΔH
GaCl$_2^{2-}$	1.988 ±0.005	1.871 ±0.005	+13.3 ±0.5	−18.9 ±0.5	+1.88 ±0.03	−1.40 ±0.05	· · ·	0.85 ±0.10
InCl$_2^{2-}$	1.886 ±0.005	1.551 ±0.005	+26.5 ±0.8	−38.7 ±0.1	+2.07 ±0.04	−1.73 ±0.08	−0.42 ±0.1	1.10 ±0.10
SnCl$_2^-$ [b] (tetrag)	1.8952 ±0.0002	1.6494 ±0.0002	+82.8 ±0.2	−93.3 ±0.6	+1.99 ±0.01	−1.43 ±0.05	· · ·	0.60 ±0.10

[a] Absolute signs determined from an analysis of the hyperfine data (see text).   [b] From Ref. 1.

for the corresponding series of divalent ns^2 metal ions in KCl. Indeed, primary SnCl$_2^-$ defects are observed in KCl:SnCl$_2$ while no PbCl$_2^-$ ESR spectra[4,5] have been found in KCl:PbCl$_2$ although here again the primary Pb$^+$ center is known to exist.[13]

The Ga⁰(4p¹) and In⁰(5p¹) on an unperturbed cation site in the KCl lattice are expected to undergo a Jahn-Teller distortion because of the threefold orbital degeneracy of the ^2P ground state. The fact that the primary Ga⁰ and In⁰ centers manifest themselves as linear symmetric GaCl$_2^{2-}$ and InCl$_2^{2-}$ molecule ions shows that the lifting of the orbital degeneracy is accompanied by the formation of the two molecular bonds.

The ESR spectra of GaCl$_2^{2-}$ and InCl$_2^{2-}$ were fitted to spin Hamiltonian (1) to which the following term (usual notation):

$$\sum_{k=1}^{2} \vec{S} \cdot \vec{a}(Cl) \cdot \vec{I}_k$$

describing the shf interaction with two equivalent chlorine nuclei, was added. The resulting ESR parameters together with the SnCl$_2^-$(tetrag) ESR data[1] are shown in Table I. The g shifts are largest for the defect with the heavier metal atom, i.e., with the larger spin-orbit coupling. The Cl shf parameters are very similar for all these centers.

C. Ga⁰(1) and In⁰(1) defects

The so called Ga⁰(1) and In⁰(1) centers[12] can be produced in two different ways. The most direct one is by x-ray irradiation of KCl:GaCl and KCl:InCl at RT. Ga⁰(1) and In⁰(1) are then produced together with other Ga⁰ and In⁰ defects; the later will be discussed in the next section. Well isolated ESR spectra of Ga⁰(1) and In⁰(1) are obtained by warming the appropriately doped KCl specimens to RT after x-ray

irradiation at 77 K. The Ga⁰(1) ESR spectra at $T = 45$ K are shown in Fig. 3. An angular variation study shows that the Ga⁰(1) ESR spectrum possesses axial symmetry around $\langle 100 \rangle$. The linewidth ΔH is somewhat anisotropic [$\Delta H(\theta = 0°) = (2.9 \pm 0.1)$ mT and $\Delta H(\theta = 45°) = (2.5 \pm 0.1)$ mT] and independent

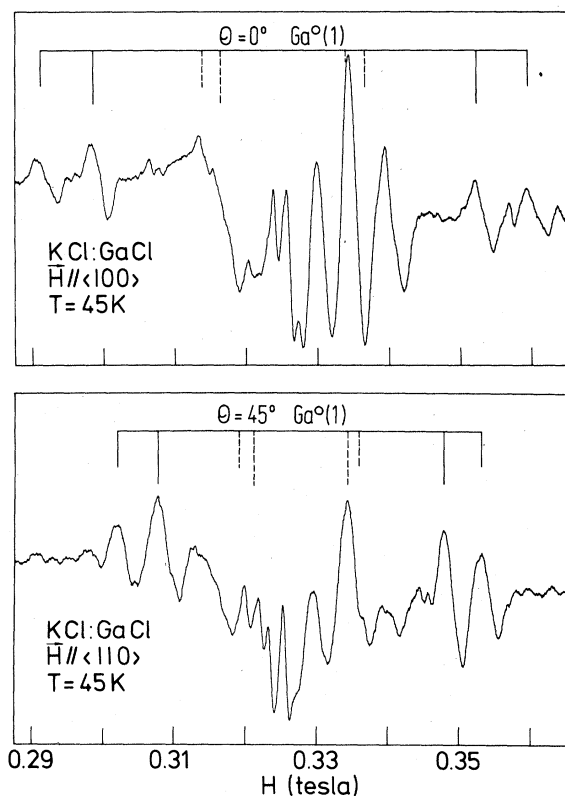FIG. 3. ESR spectra at $T = 45$ K of Ga⁰(1) in KCl:GaCl produced by x-ray irradiation at 200 K and a subsequent warmup to RT. Lines of Ga⁰(2) are also visible.
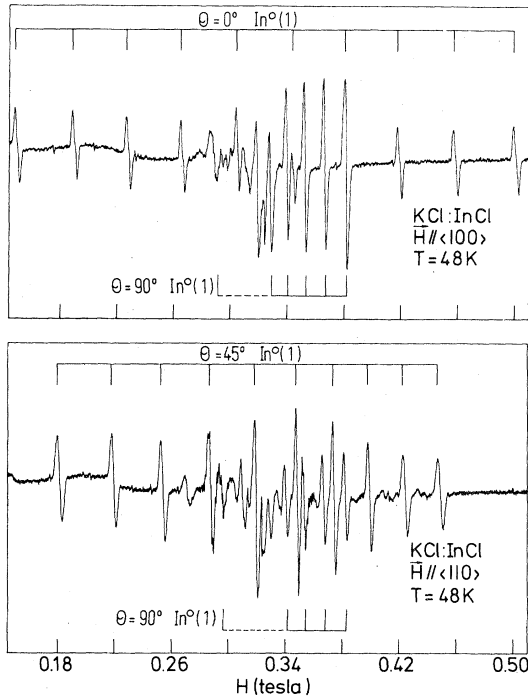
FIG. 4. ESR spectra at $T = 48$ K of $In^0(1)$ in KCl:InCl produced by x-ray irradiation at 200 K and a subsequent warmup to RT.

FIG. 5. Lowest field line of $In^0(1)$ for $\vec{H} \parallel \langle 100 \rangle$ at $T = 33$ K. The second derivative of the absorption is presented.

of the observation temperature. The large linewidth of $Ga^0(1)$ distinguishes it from the other Ga^0 centers. Close inspection of the line shape shows a hint of unresolved shf interaction.

Analogous features are observed for $In^0(1)$ whose ESR spectra at $T = 48$ K are given in Fig. 4. A careful study of the line shape clearly reveals the presence of unresolved shf structure. Figure 5 presents
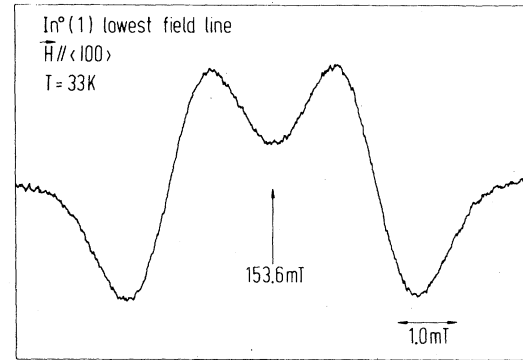
the second derivative of the lowest field line for $\vec{H} \parallel \langle 100 \rangle$. The line shape is characteristic of an unresolved shf structure consisting of several equidistant lines of equal intensity. Such a structure is in a natural way provided by the 4-line shf interaction with a single chlorine nucleus $(I = \frac{3}{2})$. A computer simulation of Fig. 5, using Gaussian line shapes and neglecting isotope effects, yields $a/\delta H \simeq 1.2$ for the ratio of the shf parameter a to the reduced linewidth δH.

The $Ga^0(1)$ and $In^0(1)$ were fitted to spin Hamiltonian (1) and the results are given in Table II. The g and hf parameters of the analogous $Tl^0(1)$ center[6] are included for comparison. The similarity of the results is readily recognized: $\Delta g_\parallel = g_0 - g_\parallel$ is smaller than $\Delta g_\perp = g_0 - g_\perp$, both shifts being largest for the atom possessing the largest spin-orbit coupling $[\xi(Ga^0) = 0.068$ eV, $\xi(In^0) = 0.199$ eV and $\xi(Tl^0) = 0.61$ eV (Ref. 14)]; $|A_\parallel|$ is larger than $|A_\perp|$. $Ga^0(1)$ and $In^0(1)$ resemble $Tl^0(1)$ in every way.

TABLE II. The spin-Hamiltonian parameters of $^{71}Ga^0(1)$ in KCl:GaCl at $T = 67$ K, of $^{115}In^0(1)$ in KCl:InCl at $T = 65$ K and of $^{205}Tl^0(1)$ in KCl:TlCl at $T = 14$ K. The hf and quadrupole parameters and the linewidth ΔH are given in mT.

Center $M^0(1)$	$g_\parallel$ [001]	$g_\perp$	$A_\parallel(M)$[a] [001]	$A_\perp(M)$[a]	$P(M)$	ΔH
$Ga^0(1)$	1.998 ±0.001	1.953 ±0.003	+23.5 ±0.1	+5.2 ±0.5	· · ·	2.7 ±0.5
$In^0(1)$	1.9837 ±0.0005	1.848 ±0.001	+38.8 ±0.1	+7.6 ±0.3	−0.47 ±0.10	3.8 ±0.5
$Tl^0(1)$[b]	1.7892 ±0.0007	1.3077 ±0.0005	+372.2[c] ±0.4	−201.1[c] ±0.2	· · ·	2.7 ±0.5

[a] Absolute signs determined from an analysis of the hyperfine data (see text).
[b] From Ref. 6.
[c] This is the traditional choice of signs. Although $A_\perp > 0$ is quoted in Ref. 6 there is no discrepancy: The phase factors in Eqs. (16) of Ref. 6 lead there to a positive sign for $A_\perp$.

D. Other Ga^0 and In^0 defects: $M^0(2)$, Ga^0 (axial) and In^0 (ortho)

A short x-ray irradiation of KCl:GaCl and KCl:InCl at RT produces besides Ga^0(1) and In^0(1) two other Ga^0 and two other In^0 centers. The ESR spectra of these centers which will be called[12] Ga^0(2) and Ga^0 (axial), and In^0(2) and In^0 (ortho), cannot be well separated from each other. Figure 6 presents the Ga^0(2) and Ga^0 (axial) spectra at 55 K. An angular variation study shows that both Ga^0 ESR spectra possess axial symmetry around $\langle 100 \rangle$. The linewidths of Ga^0(2) and Ga^0 (axial) are comparable to one another but are smaller by a factor of 3 than for Ga^0(1). A small anisotropy of ΔH is observed for Ga^0(2): $\Delta H(\theta = 0°) = (0.80 \pm 0.05)$ mT and $\Delta H(\theta = 90°) = (0.70 \pm 0.05)$ mT. For Ga^0 (axial) one finds: $\Delta H(\theta = 0°) = (0.90 \pm 0.05)$ mT and $\Delta H(\theta = 45°) = (1.10 \pm 0.05)$ mT. No motional effects, such as shifts of the ESR line positions together with a progressive line broadening are observed
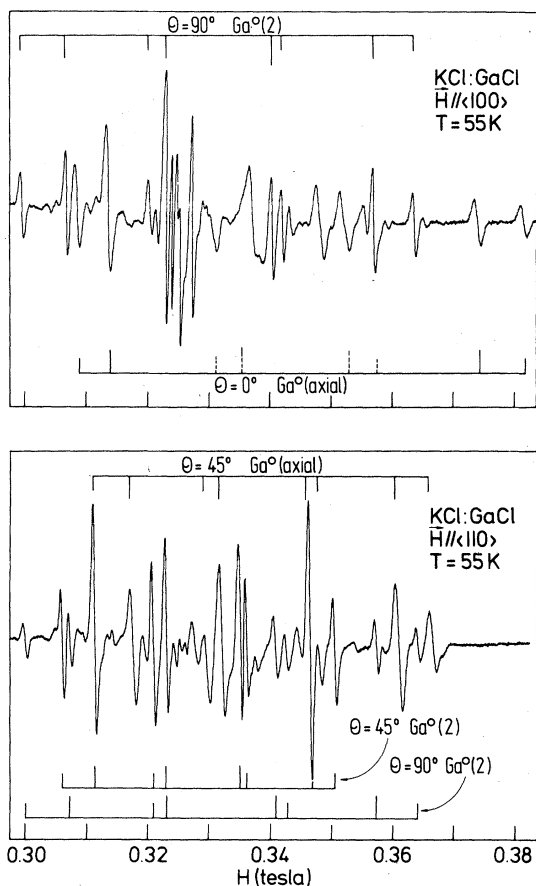
when the temperature is raised. Similarly, the Ga^0 (axial) ESR spectrum remains unchanged down to the lowest temperatures we could reach (~ 10 K).

The situation in KCl:InCl is somewhat different. In^0(2) has tetragonal symmetry around $\langle 100 \rangle$ just as Ga^0(2), but In^0 (ortho) is found to possess orthorombic symmetry with one axis along [001] and the others along [110] and [1$\overline{1}$0]. The ESR spectra of In^0(2) and In^0 (ortho) recorded at 82 K are shown in Fig. 7. In^0(1) is also visible in this figure: An obvious difference in linewidth between the three In^0 centers is readily recognized. The linewidth of In^0(2) is slightly anisotropic and about 0.8 mT; for In^0 (ortho) it is substantially larger, i.e., 1.3 mT.

The Ga^0(2) and In^0(2) defects are analogous to the Tl^0(2) defect in KCl.[6] This is clearly seen by a comparison of the spin-Hamiltonian parameters presented in Table III. For these centers one notices that $\Delta g_{\parallel} < \Delta g_{\perp}$, and $|A_{\parallel}| > |A_{\perp}|$. The latter is contrary to the hf behavior of the $M^0(1)$ defects discussed in the preceding section. In a forthcoming paper this inversion of the relative magnitude of the hf parameters will be explained by making a detailed unrestricted relativistic Hartree-Fock calculation of

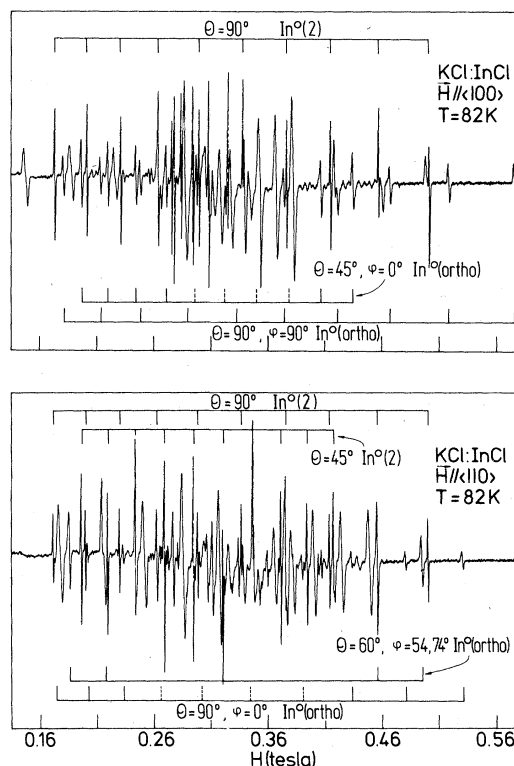FIG. 6. ESR spectra at $T = 55$ K of Ga^0(2) and Ga^0 (axial) in KCl:GaCl produced by x-ray irradiation at RT.

FIG. 7. ESR spectra at $T = 82$ K of In^0(2) and In^0 (ortho) in KCl:InCl produced by x-ray irradiation at RT. Lines of In^0(1) are also visible.

TABLE III. The spin-Hamiltonian parameters of $^{71}Ga^0(2)$ in KCl:Ga$^+$ at $T = 55$ K of $^{115}In^0(2)$ in KCl:In$^+$ at $T = 60$ K and of $^{205}Tl^0(2)$ in KCl:Tl$^+$ at $T = 14$ K. The hf and quadrupole parameters and the linewidth ΔH are given in mT.

Center $M^0(2)$	$g_{\parallel}$ [001]	$g_{\perp}$	$A_{\parallel}(M)$[a] [001]	$A_{\perp}(M)$[a]	$P(M)$	ΔH
Ga$^0(2)$	2.000 ±0.001	1.962 ±0.001	+2.2 ±0.5	−21.5 ±0.1	· · ·	0.75 ±0.05
In$^0(2)$	1.992 ±0.001	1.8872 ±0.0005	+2.5 ±0.2	−34.32 ±0.05	−0.30 ±0.10	0.80 ±0.1
Tl$^0(2)$[b]	1.8694 ±0.0007	1.4822 ±0.0004	+113.8[c] ±0.1	−415.6[c] ±0.2	· · ·	0.75 ±0.05

[a] Absolute signs determined from an analysis of the hyperfine data (see text).
[b] From Ref. 6.
[c] See footnote c in Table II.

the hf interaction including the presence of an appropriate crystal field.[6]

The ESR parameters of Ga^0 (axial) are given in Table IV. A peculiar behavior of the g values is noticed: $\Delta g_{\parallel} > \Delta g_{\perp}$. This "inversion" is explained by a motional averaging induced by a rapid reorientation motion between two equivalent planar Jahn-Teller distortions in a {100} plane (see Sec. III E).

The production and thermal properties of In^0 (ortho) and Ga^0 (axial) are very similar to each other (see Sec. V). The spin-Hamiltonian parameters of In^0 (ortho) are also given in Table IV. The deviations from axial symmetry are small. The g shifts of In^0 (ortho) are clearly larger than the shifts of the other In^0 defects.

E. Discussion of the spin-Hamiltonian parameters

1. Crystal-field model

The g and hf parameters of the various Ga^0 and In^0 defects will be discussed in terms of a simple crystal-field model.[15] The group-III metal atoms have a single p electron outside closed shells resulting in a threefold orbitally degenerate ^2P ground state. In order to describe the observed ESR parameters the defect environment is simulated by an axial crystal field. This results in the lifting of the ^2P orbital degeneracy with an energy separation E. If the crystal field, which is assumed to be much stronger than the spin-orbit interaction, is such that there is dominant

TABLE IV. The spin-Hamiltonian parameters of $^{71}Ga^0$ (axial) in KCl:Ga$^+$ at $T = 53$ K: (i) obtained from the motionally averaged ESR spectrum; and (ii) reduced to the static center data (see text), and of $^{115}In^0$ (ortho) in KCl:In$^+$ at $T = 65$ K. The hf and quadrupole parameters and linewidths ΔH are given in mT.

Center	g_z	g_x	g_y	$A_z(M)$[a]	$A_x(M)$[a]	$A_y(M)$[a]	$P(M)$	ΔH
Ga^0 (axial)[b] (i)	1.894 ±0.001	1.947 ±0.003		+23.9 ±0.5	+10.1 ±0.5		· · ·	0.95 ±0.05
Ga^0 (axial)[b] (ii)	2.000 ±0.003	1.894 ±0.001		−3.7 ±0.5	+23.9 ±0.5		· · ·	0.95 ±0.05
In^0 (ortho)[c]	1.967 ±0.003	1.806 ±0.003	1.695 ±0.003	−6.4 ±1.0	+35.7 ±0.5	+36.6 ±0.5	−0.45 ±0.15	1.3 ±0.1

[a] Absolute signs determined from an analysis of the hyperfine data (see text).
[b] For the Ga^0 (axial): $z \parallel \langle 001 \rangle$ in case (i). For case (ii) the z axis lies either along $\langle 100 \rangle$ or $\langle 110 \rangle$ in a plane perpendicular to the z axis of case (i).
[c] For the In^0 (ortho): $z \parallel [110]$, $x \parallel [001]$, and $y \parallel [1\bar{1}0]$.

attraction along the symmetry axis, z, a nondegenerate ground state is obtained: the p_z orbital is stabilized against p_x,p_y. The g components of such a system are readily calculated and up to second order in ξ/E one has

$$\Delta g_\| = g_0 - g_\| = +\frac{\xi^2}{E^2} \ , \tag{2a}$$

$$\Delta g_\perp = g_0 - g_\perp = +2\frac{\xi}{E} + \frac{\xi^2}{E^2} \ , \tag{2b}$$

with $\xi > 0$, the spin-orbit coupling constant of the np electron of Ga^0 or In^0 (see Sec. III C). The crystal-field approach is strictly valid only when there is no overlap between the metal atom and the immediate neighbors. Inclusion of overlap will modify expressions (2) considerably.[16,17]

The ground-state orbital of the metal atom is taken as

$$\Psi = \alpha|ns\rangle + \beta|np_z\rangle \ . \tag{3}$$

Even though s mixing is not always allowed because of symmetry it is included in (3) in order to be able to account formally for the isotropic hf interaction. A small amount of ns has a large influence on the hf interaction through the Fermi contact operator. To first order in ξ/E following expressions are obtained for the hf components[17]:

$$A_\| = A_\sigma + 2\rho + \tfrac{3}{2}\Delta g_\perp \rho \ , \tag{4a}$$

$$A_\perp = A_\sigma - \rho + \tfrac{13}{4}\Delta g_\perp \rho \ , \tag{4b}$$

in which the isotropic part A_σ, is

$$A_\sigma = \frac{8\pi}{3}\alpha^2 \frac{\mu_N}{I}|\Psi_{ns}(0)|^2 \ , \tag{5a}$$

and the anistropic part ρ is

$$\rho = \tfrac{2}{5}\beta^2 \frac{\mu_N}{I}\langle r^{-3}\rangle_{np} \ , \tag{5b}$$

with μ_N and I the nuclear moment and nuclear spin of the nucleus, $|\Psi_{ns}(0)|^2$ the probability density of the nucleus, $|\Psi_{ns}(0)|^2$ the probability density of the ns electron on the nucleus, and in $\langle r^{-3}\rangle_{np}$ the

average is performed over the np orbital. Exchange polarization effects can yield a negative value for A_σ.

2. Discussion of g

From the fitting of formulas (2) to the experimental g values given in Tables I–IV one can obtain an idea of the energy separation E. The results are given in Table V. The separate fitting of $g_\|$ and $g_\perp$ yields different values for E, denoted by $E_\|$ and $E_\perp$, respectively. The values of $E_\perp$ are between 50% to 200% larger than $E_\|$. This behavior points to the limited accuracy of Eqs. (2). This can have two causes.

First, $E_\|$ is obtained from the rather small second-order effects which can lead to substantial errors on the resulting numbers. Second, from the discussion of the hf parameters it will become clear that the unpaired spin density on the heavy metal atom is reduced because of covalency effects with the surroundings. Using Eq. (3) one can characterize such delocalization effects by a localization factor β^2. In fact, one can write $\beta^2 \cong f$ where f is the localization factor introduced in Ref. 6 in connection with the discussion of the g and hf components of the Tl^0(1) and Tl^0(2) defects. This delocalization lowers the value of E, and closer inspection indicates that $E_\perp$ will be reduced much more than $E_\|$. An inspection of Table V shows that the crystal-field energy separations are similar for corresponding Ga^0 and In^0 defects, being about 1 eV as measured by $E_\|$. The fact that one can describe the experimental g values by expressions (2) in a semiquantitative fashion indicates that the unpaired electron occupies a p_z orbital. For the Ga^0 (axial), the "static" g values, and for the In^0 (ortho) the g parameters in the axial approximation are used (see Secs. III E 5 and III E 6).

3. Discussion of the hf interaction

Because $\Delta g_\perp$ is experimentally known one can use expressions (4) to obtain the isotropic part A_σ and the anisotropic part ρ of the hf interaction. The signs of the hf constants $A_\|$ and $A_\perp$ cannot be determined

TABLE V. Energy separations $E_\perp$ and $E_\|$ (expressed in eV) resulting from fitting formulas (2) to the experimental $g_\perp$ and $g_\|$ values, respectively.

Center	$E_\perp$	$E_\|$	Center	$E_\perp$	$E_\|$
GaCl$_2^{2-}$	1.08	0.57	InCl$_2^{2-}$	0.97	0.58
Ga^0(1)	2.78	1.03	In^0(1)	2.65	1.46
Ga^0(2)	3.40	1.42	In^0(2)	3.55	1.95
Ga^0 (axial)	1.28	1.42	In^0 (ortho)	1.67	1.06

TABLE VI. Anisotropic part ρ and isotropic part A_σ of the hf interaction (both expressed in mT) of the various Ga^0 and In^0 centers resulting from fitting Eqs. (4) to the experimental $A_\perp$ and $A_\parallel$ values. The signs of $\gamma = A_\perp/A_\parallel$ are also given.

Center	γ	ρ^a	A_σ	Center	γ	ρ^a	A_σ
$GaCl_2{}^{2-}$	-1.42	$+9.0$	-6.3	$InCl_2{}^{2-}$	-1.46	$+12.7$	-7.4
$Ga^0(1)$	-0.22 / $+0.22^b$	$+8.9$ / $+5.7$	$+5.1$ / $+11.7$	$In^0(1)$	-0.20 / $+0.20^b$	$+12.4$ / $+8.4$	$+11.1$ / $+20.1$
$Ga^0(2)$	-9.98	$+7.4$	-13.1	$In^0(2)$	-13.73	$+10.4$	-20.0
Ga^0 (axial)	-6.46	$+7.9$	-13.3	In^0 (ortho)	$+5.65$	$+10.4$	-18.2

^{a} The free atom values are $\rho(Ga^0) = 14.8$ mT and $\rho(In^0) = 20.3$ mT (Ref. 18).
^{b} The analysis of the hyperfine data suggests that this may be the correct sign for γ.

from the ESR analysis alone. Therefore one has to investigate all sign combinations. The qualitative features of the ESR spectra and the similarity of the g shifts indicate that the localization β^2 of the unpaired electron on the Ga^0 or the In^0 should be comparable for all defects, and this should result in comparable ρ values. For $\gamma = A_\perp/A_\parallel$ negative one finds ρ values close to 8.3 and 11.5 mT for the various Ga^0 and In^0 defects, respectively (see Table VI). However, one notes that $|A_\parallel| \gg |A_\perp|$ for $Ga^0(1)$ and $In^0(1)$ and taking γ positive in this case does not alter too drastically the ρ value as Table VI shows. Thus it is concluded that $\gamma = A_\perp/A_\parallel$ is negative for all the Ga^0 and In^0 defects, except maybe for $Ga^0(1)$ and $In^0(1)$ where $\gamma > 0$ remains a possibility. In a forthcoming paper[18] where the results of a relativistic many-body calculation of the Ga^0 and In^0 hf structure will be presented it will be argued that the last sign combination for $Ga^0(1)$ and $In^0(1)$ could be the correct one. In the same paper values are obtained for ρ of the free Ga^0 and In^0 atoms, i.e., $\rho(Ga^0) = 14.8$ mT and $\rho(In^0) = 20.3$ mT. Using these values in Eqs. (5) together with the experimental data of Table VI yields the following localization factors: $\beta^2 = 0.61$, 0.39, 0.50, and 0.53 for $GaCl_2{}^{2-}$, $Ga^0(1)$, $Ga^0(2)$ and Ga^0 (axial), respectively. Similarly one finds $\beta^2 = 0.63$, 0.41, 0.51, and 0.51 for $InCl_2{}^{2-}$, $In^0(1)$, $In^0(2)$, and In^0 (ortho). These localization factors are somewhat smaller than the f values to be presented in Ref. 18 but they show the same trend and variation.

The A_σ values are also given in Table VI. A striking feature are the large positive A_σ values for the $Ga^0(1)$ and $In^0(1)$ defects irrespective of the sign chosen for $\gamma = A_\perp/A_\parallel$. This is probably due to a strong first-degree field which results in a substantial positive contribution to the isotropic hf interaction through the mixing of ns into np_z. An important observation which has a bearing on the models of the Ga^0 and In^0 defects is that the magnitude and sign of

A_σ seems to reflect on whether or not the impurity atom has a defect environment possessing inversion symmetry.

4. Discussion of the Cl shf interaction

In the same way as the Ga^0 and In^0 hf parameters were discussed, the Cl shf constants of the $GaCl_2{}^{2-}$ and $InCl_2{}^{2-}$ defects can be handled. In Table VII the isotropic part a_σ and the anisotropic part ρ of the Cl shf interaction are given for $a_\perp/a_\parallel$ positive and negative. Expressions (4) are used with $\Delta g_\perp = 0$. If $a_\perp/a_\parallel$ is taken to be positive than ρ is around 0.15 mT. This can be compared to the ρ of the $Cl_2{}^-$ V_K center which is 3.23 mT in KCl.[17] It is concluded that for this choice of sign about 5% of the electron spin density is on the chlorines and 95% is on the central metal atom. If, however, $a_\perp/a_\parallel$ is taken to be negative, ρ is around 1.2 mT and only 70% of the unpaired electron spin density is on the Ga^0 or In^0. This latter choice of sign is considered to be the correct one because it agrees with the localization factor $\beta^2 \approx 0.6$ obtained in Sec. III E 3.

TABLE VII. Anisotropic part ρ and isotropic part a_σ of the chlorine shf interaction (expressed in mT) resulting from fitting Eqs. (4) to $a_\perp$ and $a_\parallel$ of $GaCl_2{}^{2-}$ and $InCl_2{}^{2-}$ for $\gamma = a_\perp/a_\parallel$ positive and negative. The latter is argued to be the correct sign. $SnCl_2{}^-$ data are included for comparison.

Center	$\gamma > 0$		$\gamma < 0$	
	ρ	a_σ	ρ	a_σ
$GaCl_2{}^{2-}$	$+0.16$	$+1.56$	$+1.09$	-0.31
$InCl_2{}^{2-}$	$+0.11$	$+1.84$	$+1.27$	-0.46
$SnCl_2{}^-$ (tetrag)	$+0.19$	$+1.62$	$+1.14$	-0.29

5. Ga^0 (axial)

As pointed out in Sec. III D the Ga^0 (axial) center has the unusual property that $\Delta g_{\parallel}$ is larger than $\Delta g_{\perp}$. There is no way to explain this except if one accepts that a fast internal motion occurs between two equivalent positions in a plane perpendicular to an axis which, in the frozen in or static center, corresponds to a $g_{\perp}$ or an $A_{\perp}$ direction. The g and A parameters of Ga^0 (axial) as measured from the ESR spectra are then motionally averaged values, which are here denoted by $\langle g \rangle$ and $\langle A \rangle$. They can be expressed as a function of the parameters of the static center:

$$\langle g_{\parallel} \rangle = g_{\perp,sta} \ , \quad \langle g_{\perp} \rangle = \tfrac{1}{2}(g_{\parallel,sta} + g_{\perp,sta}) \ , \qquad (6)$$

with analogous formulas for $\langle A \rangle$. The spin-Hamiltonian parameters for the static center can be deduced from Eqs. (6). One obtains $g_{\parallel,sta} = 2.000$ and $g_{\perp,sta} = 1.894$. These are comparable to the g values of the other Ga^0 centers which lends support to our interpretation. The determination of the static hf parameters is somewhat less straightforward as the sign of $\langle A \rangle$ cannot be determined from the ESR analysis. If the signs of $\langle A_{\parallel} \rangle$ and $\langle A_{\perp} \rangle$ are different one obtains $|A_{\parallel,sta}| = 44.1$ mT and $|A_{\perp,sta}| = 23.9$ mT. If $\langle A_{\parallel} \rangle$ and $\langle A_{\perp} \rangle$ possess the same sign, then $|A_{\parallel,sta}| = 3.7$ mT and $|A_{\perp,sta}| = 23.9$ mT. The latter parameters are accepted as being the correct ones because their sizes are more in line with those of the other Ga^0 defects and because their analysis gives the most reasonable ρ and A_{σ} values.

6. In^0 (ortho)

Deviations from axial symmetry of the In^0 (ortho) spin-Hamiltonian parameters are small. In the discussion of the g and hf constants, the parameters resulting from an axial approximation are used: $g_{\perp} = \tfrac{1}{2}(g_x + g_y)$ and $A_{\perp} = \tfrac{1}{2}(A_x + A_y)$.

IV. MODELS FOR THE Ga^0 AND In^0 DEFECTS

A. Primary Ga^0 and In^0 centers: $GaCl_2^{2-}$ and $InCl_2^{2-}$

The model for the primary Ga^0 and In^0 centers can be derived from the ESR data. It is depicted in Fig. 8(a) for the Ga^0 case; it consists of a linear symmetric $\langle 100 \rangle$ oriented $(Cl^-Ga^0Cl^-)$ molecule ion with no perturbing defect in the neighborhood. Note in passing that the $Ga^0(4p^1)$ is perfectly on center here in contrast to the Ga^+ in its excited $4s4p$ state.[11] The model is identical to the one proposed for the $SnCl_2^-$(tetrag) center in $KCl:SnCl_2$.[1] The ground

molecular orbital of $GaCl_2^{2-}$ is composed out of a $4p_z$ function on the Ga^0 and two s-p hybrids, one on each Cl^- ion, forming a bonding σ_u type orbital.[1,16] The bond-switching internal motion of the primary $GaCl_2^{2-}$ and $InCl_2^{2-}$ defect indicated by the temperature dependence of the ESR spectra is also allowed by the model of Fig. 8(a). Because there is no perturbing defect in the immediate neighborhood of the molecule ion every $\langle 100 \rangle$ direction is equivalent, and a three-dimensional jumping motion between the three $\langle 100 \rangle$ direction can occur.

If the bond-switching motion is a normal thermally activated process it is described by

$$R = se^{-\Delta E/kT} \qquad (7)$$

with R the reorientation frequency of the $GaCl_2^{2-}$ or $InCl_2^{2-}$ defect, s the frequency factor, and ΔE the activation energy. At the temperature that the linewidth starts to broaden, i.e., at 25 K for $GaCl_2^{2-}$ and around 10 K for $InCl_2^{2-}$, R is about 5×10^6 Hz.[19] Taking $s \cong 1 \times 10^{12}$ Hz as a representative frequency factor one calculates ΔE from Eq. (7) to be ~ 0.028 eV for $GaCl_2^{2-}$ and ~ 0.011 eV for $InCl_2^{2-}$. Both activation energies are low. If ΔE is known one can estimate the temperature at which the motion freezes in. For $GaCl_2^{2-}$ this is around 10 K, and for $InCl_2^{2-}$ this temperature is in the neighborhood of 4.2 K. One may wonder, especially in the case of $InCl_2^{2-}$, whether it is still possible to have an Arrhenius type motion at such low temperatures. It is more likely that one is dealing with a one or two phonon-assisted tunneling motion. Polarized optical absorption measurements and uniaxial stress experiments at liquid-helium temperatures may clarify this matter.
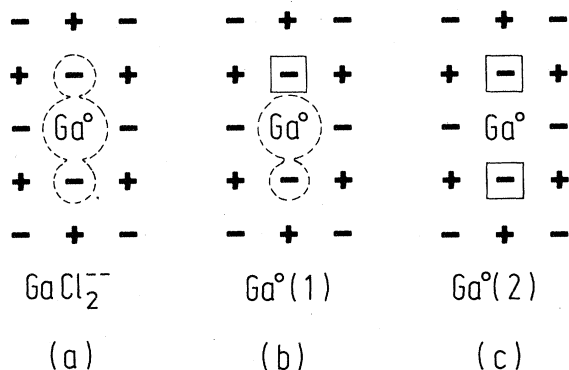

FIG. 8. Schematic two-dimensional models of the MCl_2^{2-}, $M^0(1)$ and $M^0(2)$ centers. Shown are (a) the primary $GaCl_2^{2-}$, (b) $Ga^0(1)$, and (c) $Ga^0(2)$. The primary MCl_2^{2-} manifests itself as a linear symmetric molecule ion. This is indicated by the dotted line.

B. $Ga^0(1)$ and $In^0(1)$ centers

The ESR data strongly imply that $Ga^0(1)$ and $In^0(1)$ possess the same defect structure. In Fig. 8(b) the model for $Ga^0(1)$ is depicted: it is identical to the $Tl^0(1)$ model.[6] It consists of a Ga^0 on a cation site with a single negative ion vacancy in a nearest-neighbor position along a $\langle 100 \rangle$ direction. Supporting evidence for this structure is furnished by the observed shf interaction with a single chlorine nucleus (see Fig. 5) provided by the substitutional Cl^- [indicated inside the dotted line in Fig. 8(b)]. The assumption that a single negative-ion vacancy is involved is further based on production, isothermal, and isochronal pulse anneal experiments (Sec. V). The observed $\langle 100 \rangle$ axial symmetry is further determined by the negative ion vacancy.

C. $Ga^0(2)$ and $In^0(2)$ centers

The model of $Ga^0(2)$ and $In^0(2)$ is presented for the former in Fig. 8(c). It is identical to the $Tl^0(2)$ model.[6] The impurity atom, on a cation lattice site, is flanked by two negative ion vacancies in a $\langle 100 \rangle$ direction. The model has the correct symmetry: tetragonal around $z \parallel \langle 100 \rangle$. The narrow ESR lines are explained by the fact that the $\langle 100 \rangle$ oriented p_z lobe of the impurity atom does not overlap with any chlorines. The presence of negative ion vacancies is further supported by several production and thermal anneal experiments (see Sec. V).

A confirmation for the proposed models for the Tl^0 defects could be gotten from relativistic many body calculations of the hf interactions including the effect of an appropriate electrostatic potential. It was shown that a first-degree crystal field gives $|A_{\parallel}| > |A_{\perp}|$ and a second-degree field yields $|A_{\parallel}| < |A_{\perp}|$ corresponding to the experimentally observed behavior of the hf parameters of $Tl^0(1)$ and $Tl^0(2)$, respectively.[6] A first-degree field is provided by a single negative-ion vacancy and two negative-ion vacancies alongside the impurity induce a second-degree field only; this confirms the proposed defect structures. Analogous calculations to be presented in a forthcoming paper[18] lead to the same results for Ga^0 and In^0 defects.

D. Ga^0 (axial)

In Sec. III D it was shown independent of any model for the Ga^0 (axial) center that its observed g components could only be explained by a rapid reorientation motion between two equivalent orientations in a $\{100\}$ plane. The observed motionally averaged g and A constants were transformed into static center data corresponding to axial symmetry

with a z axis in a $\{100\}$ plane. Although this must represent an approximation to orthorhombic symmetry, it was no hindrance in the formal analysis of the hf components, the results of which are given in Table VI. In searching for models for Ga^0 (axial) one must consider only those that permit a motion confined to a $\{100\}$ plane.

Figure 9(a) presents a simple model in which a Ga^0 on a positive ion site is perturbed by a next-nearest-neighbor (NNN) positive ion vacancy, $(+)$, along $\langle 100 \rangle$. This model which allows a motion in a $\{100\}$ plane perpendicular to the $Ga^0 - (+)$ axis is not acceptable as the following arguments show. The structure in Fig. 9(a) is identical to the well established[1] structure of the Sn^+ $(+, NNN)$ center shown in Fig. 10(b). Such a center manifests itself as a $SnCl_2^-$ molecule ion whose molecular axis, z, is perpendicular to the $\{100\}$ plane of the figure. The NNN positive ion vacancy represents a *weak* perturbation, just enough to induce the observed orthorhombic symmetry of the Sn^+ $(+, NNN)$ center with the x and y axes along perpendicular $\langle 100 \rangle$ directions. Consequently, for the proposed model in Fig. 9(a) one would expect to see a $GaCl_2^{2-}$ molecule ion with the molecular axis z perpendicular to the plane of the figure and possessing a small orthorhombic distortion induced by the positive-ion vacancy. This is not observed even at ~ 10 K. The Sn^+ $(+, NNN)$ center is known to possess a motion between two equivalent $\langle 100 \rangle$ orientations in a $\{100\}$ plane perpendicular to the $Sn^+ - (+)$ axis, the so-called "propeller" motion.[1] The activation energy for this motion is virtually identical to the one of the unperturbed Sn^+ (tetrag) center [see Fig. 10(c)] which has a structure identical to the primary $GaCl_2^{2-}$ center. One expects a similar behavior for the $GaCl_2^{2-}$ centers. Because as shown in Sec. IV A, the primary $GaCl_2^{2-}$ center is frozen in at 10 K, one expects the same for the model in Fig. 9(a). Thus for this structure no rapid
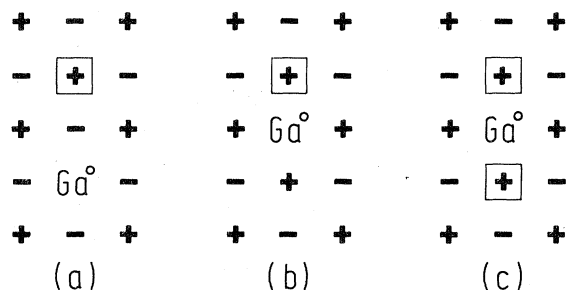

FIG. 9. Schematic representation of three possible models of Ga^0 (axial). In the favored models (b) and (c) the Ga^0 atom is located on an anion site. The building blocks in (b) are the same as for $Ga^0(1)$ in Fig. 8(b), and the same holds for (c) and the In^0 (ortho) model in Fig. 11(c). Model (a) is argued to be an unacceptable one.
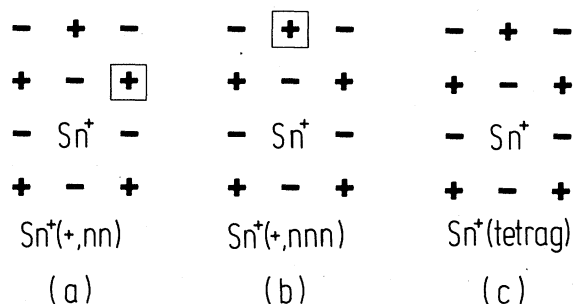
```
- +  -        - +̄ -        - +  -
+ -  +̄        + - +        + - +
- Sn⁺ -       - Sn⁺ -      - Sn⁺ -
+ - +         + - +        + - +

Sn⁺(+,nn)     Sn⁺(+,nnn)   Sn⁺(tetrag)

  (a)           (b)          (c)
```

FIG. 10. Schematic two-dimensional models for (a) Sn^+ (+,NN), (b) Sn^+ (+,NNN), and (c) Sn^+ (tetrag). The Sn^+ defects manifest themselves as linear symmetric $SnCl_2^-$ molecules; the molecular axis is oriented perpendicular to the plane of the figure (from Ref. 1).

reorientation motion at 10 K is expected to occur, which would be necessary to produce motionally averaged ESR parameters. Another reason for rejecting the model in Fig. 9(a) is that Sn^+ (+,NNN) possesses a lower thermal stability than Sn^+ (tetrag), while one would have to have to accept the opposite for the corresponding $GaCl_2^{2-}$ centers (see Sec. V).

Another possible model for Ga^0 (axial) is presented in Fig. 9(b): A Ga^0 on an anion site is perturbed by a nearest-neighbor (NN) positive ion vacancy. The building blocks of this model are the same as for the $Ga^0(1)$ center presented in Fig. 8(b), but in Fig. 9(b) the Ga^0 occupies the negative ion vacancy. If this model is correct then each vacancy must define a potential well for the Ga^0 both separated by a sufficiently large potential barrier. One of the positions will be an absolute minimum and if the potential barrier can be crossed one configuration will be converted into the other. The pulse anneal data to be presented later in Sec. V show that Ga^0 (axial) possesses lower thermal stability than $Ga^0(1)$. One observes that because of its narrower linewidth Ga^0 (axial) is present in a much smaller amount than $Ga^0(1)$. Thus its decay may not result in an observable increase of the $Ga^0(1)$ intensity. Furthermore, the two decay temperatures are sufficiently close together so that any formation of $Ga^0(1)$ out of Ga^0 (axial) may already be overwhelmed by its own thermal decay.

Figure 9(c) presents another possibility for Ga^0 (axial). Here a Ga^0 on a negative ion site is flanked by two positive ion vacancies along $z \parallel \langle 100 \rangle$. Just as in the previous model, the negatively charged cation vacancies raise the energy of the p_z level, leaving a twofold orbitally degenerate $\{p_x, p_y\}$ set in the $\{100\}$ plane perpendicular to z axis defined by the two vacancies. A planar Jahn-Teller distortion will lift this degeneracy and very likely the resulting ground orbital will be oriented along a $\langle 110 \rangle$. If the energy bar-

rier between the two equivalent $\langle 110 \rangle$ distortions in the $\{100\}$ plane is sufficiently small, a fast phonon-assisted jumping motion may occur between them producing a motionally averaged ESR spectrum. An argument against this model (but favoring the foregoing one) is that two positive ion vacancies are required. If Fig. 9(c) represents the true model then one has to accept either that cation vacancies are grown into the crystal as charge compensators for oxidized impurities such as Ga^{3+}, or that a sizable amount of Ga^- centers on anion sites have been produced which have released the positive ion vacancy originally occupied by the Ga^+.

F. In⁰ (ortho) center

The production and decay properties of the Ga^0 (axial) and In^0 (ortho) centers to be presented in Sec. V are very similar to each other and this could suggest a similar structure for both. Moreover, the ESR parameters also show an analogous behavior as can be seen from Tables V and VI. In the foregoing subsection it was argued that Ga^0 (axial) is in essence an orthorhombic center but because of motional averaging in a $\{100\}$ plane it looks like an axial center. In fact one can propose for In^0 (ortho) the same models as presented for Ga^0 (axial) in Figs. 10(b) and (c) but with the understanding that the two-dimensional Jahn-Teller effect in the $\{100\}$ plane is a strong one, localizing the ground state into a $\langle 110 \rangle$ direction even at temperatures as high as the In^0 (ortho) decay temperature. However, the absence of observable motional effects for In^0 (ortho) may equally well mean that its structure does not permit them, which raises the question why no defect analogous to Ga^0 (axial) is observed in $KCl:In^+$.

Figures 11(a)–11(c) present therefore a few other models for In^0 (ortho) which appear possible and reasonable. The difference between the models of Figs. 11(a) and 11(b) is the presence of a positive ion vacancy in the $\langle 110 \rangle$ direction of Fig. 11(b). The model of Fig. 11(a) puts the In^0 on a cation site and uses only negative ion vacancies. If this model is the correct one, one must accept that two different configurations of the negative ion vacancies around the In^0 can exist, because the building blocks of the model in Fig. 11(a) are the same as for the linear $In^0(2)$ model shown in Fig. 8(c). If the positive ion vacancy is also present [see Fig. 11(b)] it can act as a glue reducing the repulsion between the two negative ion vacancies. In both cases the In^0 has to move to the symmetric position in order to obtain the correct orthorhombic symmetry: the In^0 must lie off center exactly half way between the negative ion vacancies. The model of Fig. 11(c) is in a sense the opposite of Fig. 11(b): the positive ion vacancies are replaced by negative ones and vice versa. Notice again that the
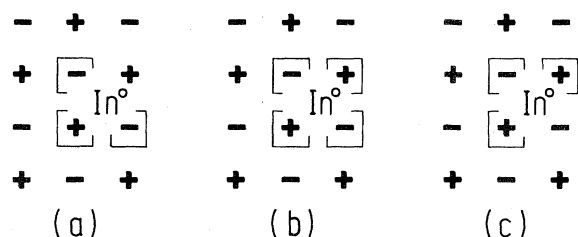
FIG. 11. Schematic representation of three possible models of In^0 (ortho); still other models are discussed in the text. The In^0 atom is in a symmetric off-center position in the three cases. In (a) the building blocks are the same as for $In^0(2)$ in Fig. 8; in (c) they are the same as for Ga^0 (axial) in Fig. 9(c).

FIG. 12. Production at 77 K of the primary In^0 defect in KCl:InCl as a function of the x-ray irradiation time. The primary $GaCl_2^{2-}$ defect in KCl:GaCl behaves analogously. Formation of the V_k center is also indicated.

building blocks of the model in Fig. 11(c) are the same ones as used in Fig. 9(c) which is one of the two proposed models for Ga^0 (axial).

Another simple and possible In^0 (ortho) model not presented in a figure is an In^0 atom on an unperturbed *anion* site. Such a system must undergo a Jahn-Teller distortion and if this would be an orthorhombic one with at least one axis along $\langle 110 \rangle$ then this model could be an acceptable one. Only detailed calculations will be able to substantiate or refute this model.

One can also construct models with an In^0 on an anion site either associated with one, or flanked by two anion vacancies along $\langle 110 \rangle$. Because these models involve only anion vacancies, repulsive forces will be strong and it seems unlikely that these would represent stable centers. The ESR data already discussed and the production and thermal data to be presented in Sec. V have not permitted us to be more specific and the In^0 (ortho) model is still much an open question.

V. PRODUCTION AND THERMAL PROPERTIES OF THE Ga^0 AND In^0 DEFECTS

A. Formation of the primary $GaCl_2^{2-}$ and $InCl_2^{2-}$ by x-ray irradiation at 77 K

X-ray irradiation of KCl:GaCl and KCl:InCl at 77 K produces besides, e.g., the V_K center,[17,20] the primary $GaCl_2^{2-}$ and $InCl_2^{2-}$. Only a small amount of Ga^{2+} and In^{2+} defects are formed; most of the holes released in the crystal are trapped as V_K centers.

The formation of the primary $GaCl_2^{2-}$ and $InCl_2^{2-}$ was studied as a function of the x-ray irradiation time at 77 K. The results are depicted in Fig. 12 for $InCl_2^{2-}$. The rate of formation of $InCl_2^{2-}$ is high at the beginning of the irradiation. After about 20 min the production of $InCl_2^{2-}$ levels off. The production
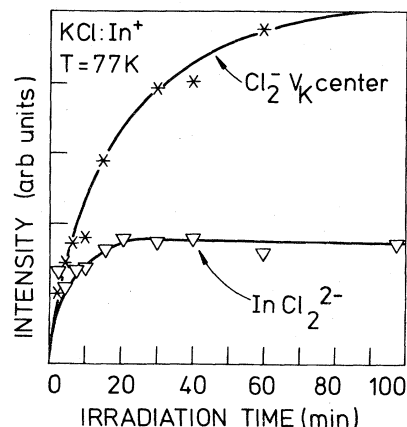
curve for the Cl_2^- V_K center is also presented and a rapid growth within the first 10 min of the irradiation is observed. $GaCl_2^{2-}$ behaves similarly to $InCl_2^{2-}$.

Because $GaCl_2^{2-}$ and $InCl_2^{2-}$ are produced in large quantities by short x-ray irradiations below 230 K it is concluded that the formation proceeds by direct trapping of an electron by a substitutional Ga^+ or In^+. Indeed, interstitial chlorine ions or atoms have a much slower production rate (by about an order of magnitude) than electrons and furthermore negative and positive ion vacancies are not mobile below 230 K.[6,21]

B. Formation at RT of the various Ga^0 and In^0 centers as a function of the x-ray irradiation time

In order to study the production of Ga^0 and In^0 defects obtained by x-ray irradiation at RT an experiment similar to the one described in the foregoing section was performed. Figure 13 gives the production curve of $In^0(1)$, $In^0(2)$, and In^0 (ortho) as a function of the x-ray irradiation time at RT. All In^0 centers are initially rapidly formed by x-ray irradiation. The $In^0(1)$ concentration reaches a maximum at about 12 min, after which it decays slowly. The rate of formation of $In^0(2)$ is slightly lower than of $In^0(1)$. The $In^0(2)$ intensity reaches a saturation value after about 20 min. For In^0 (ortho) a somewhat slower production rate is observed. More than half of the In^0 (ortho) defects, are created within the first 20 min of the irradiation. The formation characteristics of the Ga^0 centers are similar to those of the In^0 centers. In particular the production curve of Ga^0 (axial) behaves similarly to that of In^0 (ortho), possi-

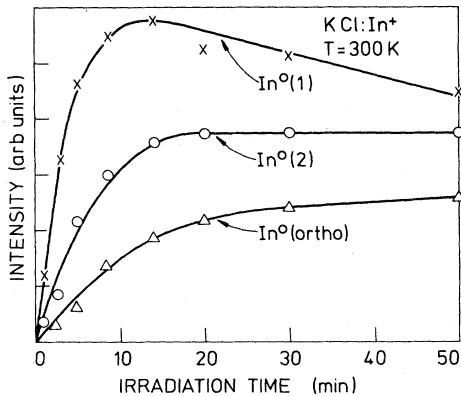FIG. 13. Production at RT of In^0(1), In^0(2), and In^0 (ortho) as a function of the x-ray irradiation time. The formation of Ga^0(1), Ga^0(2), and Ga^0 (axial) proceeds analogously.

FIG. 14. Production of In^0(1), In^0(2), In^0 (ortho), and the primary InCl$_2$$^{2-}$ in KCl:InCl as a function of the x-ray irradiation temperature. After quenching the specimen from 400 °C it was x-ray irradiated for 15 min at every measuring temperature. The same experiment on KCl:GaCl leads to analogous results.

bly pointing to a similar formation mechanism for both defects.

The models presented in Sec. IV are in agreement with the experimental results. The somewhat slower production rate of In^0(2) and In^0 (ortho) compared to In^0(1) is due to the following: (i) the creation of In^0(2), and maybe also In^0 (ortho), requires a reasonable In^0(1) concentration; and (ii) the availability of a second negative or a positive ion vacancy. In^0(1) can be formed in two different ways: trapping of an electron by the impurity metal ion and a subsequent stabilization of a negative ion vacancy or vice versa. It is possible that both processes occur.

C. Production of Ga^0 and In^0 centers by x-ray irradiation at various temperatures

To get further information on the production mechanism of the Ga^0 and In^0 centers the following experiment was performed. At successive temperatures between 220 and 340 K the appropriately doped KCl crystal was x-ray irradiated for 15 min. After each x-ray irradiation the ESR intensities of the Ga^0 and In^0 centers were recorded. Before each cycle of the experiment the initial state of the crystal was restored by heating the crystal to about 400 °C and quickly quenching it to RT. The results are shown in Fig. 14 for KCl:InCl. Several features are apparent: (i) InCl$_2$$^{2-}$ is only formed by x-ray irradiation at "low" temperatures, i.e., between 77 and 250 K; (ii) the onset temperatures of formation of In^0(1), In^0(2), and In^0 (ortho) are above all 230 K, respectively, at 240, 260, and 290 K; (iii) the distinct maximum production temperatures are at about 280 K for In^0(1) and In^0(2), but at 300 K for In^0 (ortho); and (iv) no In^0 centers are formed in appreciable

amounts above 330 K. Essentially the same features are found if the experiment is repeated on KCl:GaCl.

The experimental observations are in agreement with the models proposed for the Ga^0 and In^0 defects. Specifically, because it is assumed that a negative ion vacancy is part of the In^0(1), In^0(2), and maybe also the In^0 (ortho) defect structure, these centers are only produced above 230 K, the temperature at which negative ion vacancies become mobile. A higher onset formation temperature of In^0(2) and In^0 (ortho) is reasonable if we recognize that the production of both centers involves a certain amount of In^0(1) and the occurrence of a secondary process such as the trapping of a second negative ion vacancy. Here it is implied that In^0(1) is the intermediate step in the formation of In^0(2) and In^0 (ortho). In^0(1) is electrically neutral and consequently it can trap negative as well as positive ion vacancies. A jump of the atom into the negative ion vacancy could occur at high temperatures. The decay of the In^0 defects above 300 K could be due to processes such as trapping of an electron leading to In$^-$ centers which are diamagnetic and not observable in ESR.

D. Pulse anneal experiment after x-ray irradiation at 77 K

Figure 15 presents a pulse anneal experiment between 190 and 310 K of KCl:GaCl irradiated at 77 K for 15 min. This treatment produces among other defects, GaCl$_2$$^{2-}$ and V_K centers.[17,20] Around 210 K the V_K center decays and the resulting mobile holes are retrapped mostly by Ga$^+$ impurities to form[22] Ga^{2+} (not shown on the figure) and some by GaCl$_2$$^{2-}$. The former process explains why the drop
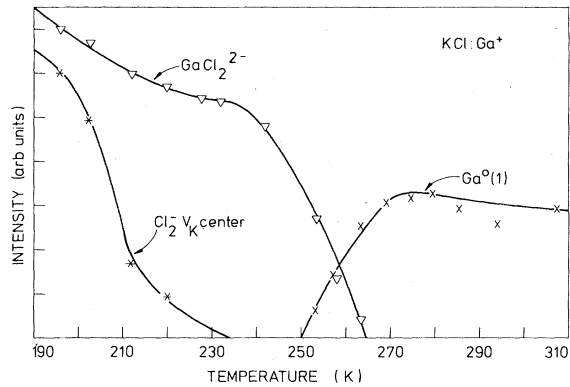
FIG. 15. Pulse-anneal experiment between 190 and 310 K on a KCl:GaCl specimen which was x-ray irradiated at 77 K for 15 min. The crystal was held for 5 min at every measuring temperature.

in intensity of $GaCl_2^{2-}$ between 200 and 240 K is rather small. Above 240 K $GaCl_2^{2-}$ becomes thermally unstable, the electrons released in the crystal are partly trapped by Ga^{2+} restoring some of the initial Ga^+ concentration.

Yet another process can happen. Negative ion vacancies which have been created by a short x-ray irradiation at 77 K, as the complementary reaction product of interstitial chlorine ion formation, become mobile above 230 K and are trapped by $GaCl_2^{2-}$. This results in a further decay of $GaCl_2^{2-}$ and the formation of $Ga^0(1)$ between 250 and 270 K. Further heating of the crystal does not produce other Ga^0 defects. Only a small amount of $Ga^0(1)$ is formed by this procedure probably, (i) because most of the $GaCl_2^{2-}$ have thermally decayed around 260 K and a lot of $GaCl_2^{2-}$ is lost in the production of $Ga^0(1)$, and (ii) because only a limited number of interstitial chlorine ions and thus a limited number of negative ion vacancies are produced by the short x-ray irradiation at 77 K. The latter might also explain why only $Ga^0(1)$ is produced.

If a pulse anneal was performed on KCl:GaCl which was x-ray irradiated at 220 K then $Ga^0(2)$ is produced in sizable amounts (see Fig. 16). This is probably because of a higher production of negative ion vacancies by the x-ray irradiation at 220 K. In this annealing experiment one also observes a higher onset temperature of formation of $Ga^0(2)$ compared to $Ga^0(1)$, in general agreement with production data presented in foregoing sections. It is noteworthy that Ga^0 (axial) is not produced by this procedure.

Analogous pulse anneal experiments on KCl:InCl x-ray irradiated at low temperatures (<230 K) do not lead to higher concentrations of In^0 defects. A subsequent optical bleaching of the F centers, however, yields the $In^0(1)$ ESR spectrum. This indicates
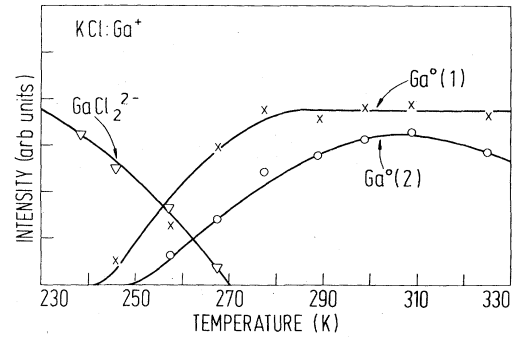
FIG. 16. Pulse-anneal experiment between 230 and 330 K on a KCl:GaCl specimen after x-ray irradiation at 220 K for 15 min.

that a precursor center exists consisting of an In^+ and a single negative ion vacancy in a nearest-neighbor position. Such type of a precursor center, which may be called $In^+(1)$,[12] was also identified in KCl:Tl$^+$.[6]

E. Isothermal anneal at different temperatures after x-ray irradiation at 77 K

In order to establish more clearly the relation between $GaCl_2^{2-}$ and $Ga^0(1)$ and to illustrate the role of negative ion vacancies in the formation of $Ga^0(1)$ the following experiment was performed. After a 15 min x-ray irradiation at 77 K of KCl:GaCl two isothermal anneals at, respectively, 230 and 245 K were performed. The temperatures were chosen in this region, where the negative ion vacancies become mobile.

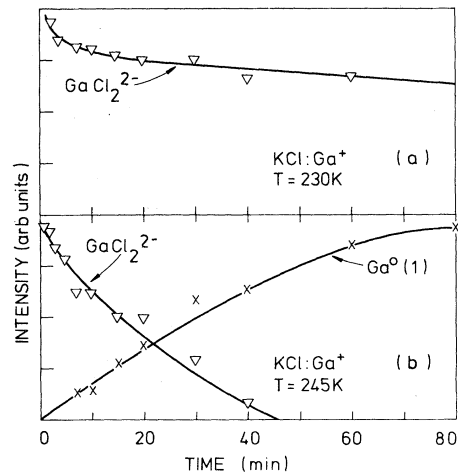The results are given in Fig. 17. The anneal at 230

FIG. 17. Two isothermal anneals of a KCl:GaCl specimen which was x-ray irradiated for 15 min at $T = 77$ K. (a) $T = 230$ K and, (b) $T = 245$ K, i.e., in the temperature region where negative ion vacancies become mobile.

K [Fig. 15(a)] shows that $GaCl_2^{2-}$ decays slowly very likely because of its own thermal instability, i.e., it loses an electron. No $Ga^0(1)$ defects are formed: the negative ion vacancies are not yet sufficiently mobile. If the annealing temperature is 245 K [Fig. 15(b)] then $GaCl_2^{2-}$ decays more rapidly (half of maximum intensity is reached in about 17 min) and $Ga^0(1)$ is now formed (half of maximum intensity after about 23 min), pointing to the availability of mobile negative ion vacancies, which are trapped by $GaCl_2^{2-}$ and form $Ga^0(1)$.

F. Pulse anneal experiment after x-ray irradiation at RT

A short x-ray irradiation of KCl:InCl at RT produces $In^0(1)$, $In^0(2)$, and In^0 (ortho). A pulse anneal experiment between 310 and 450 K was performed in order to establish the thermal stabilities of the In^0 centers. The results are depicted in Fig. 18. It is noticed that the various In^0 defects decay at substantially different temperatures. In^0 (ortho) is produced only by x-ray irradiation above 290 K and its decay temperature is around 335 K. The $In^0(2)$ defect disappears around 370 K. The decay of $In^0(1)$ proceeds in two steps. Between 350 and 380 K a pronounced drop of the $In^0(1)$ concentration is noticed, but at still higher temperatures (440 K) the final disappearance is observed. The first step at 365 K must involve the decay of another defect not observable in ESR.

A similar experiment was performed on KCl:GaCl. The same qualitative features for the decay of $Ga^0(1)$, $Ga^0(2)$, and Ga^0 (axial) are observed. In particular it is noticed that the decay temperature of Ga^0 (axial) corresponds to that of In^0 (ortho).

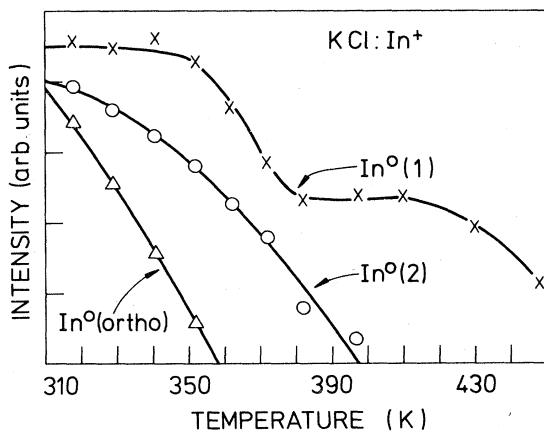FIG. 18. Pulse-anneal experiment between 310 and 450 K of a KCl:InCl sample which was x-ray irradiated for 15 min at RT to produce $In^0(1)$, $In^0(2)$, and In^0 (ortho). Analogous results are obtained for KCl:GaCl.

VI. CONCLUDING REMARKS

The fact that the ESR spectra of the primary $Ga^0(4p^1)$ and $In^0(5p^1)$ centers are observed and that they show up as $\langle 100 \rangle$ oriented symmetric and linear $GaCl_2^{2-}$ and $InCl_2^{2-}$ molecular ions is interesting because the ESR spectrum of the primary $Tl^0(6p^1)$ center has so far eluded detection. The observed properties of $GaCl_2^{2-}$ and $InCl_2^{2-}$ may throw some light on this matter. First it is noticed that the best ESR observation temperature is lower for $InCl_2^{2-}$ than for $GaCl_2^{2-}$, suggesting, if this trend can be extrapolated, that for the primary Tl^0 even lower observation temperatures are required. However, even at 2 K the primary Tl^0 ESR spectrum was not detected.[23] More important may be the observation that both $GaCl_2^{2-}$ and $InCl_2^{2-}$ possess a reorientation motion, a bond switching among the three $\langle 100 \rangle$ directions. For $InCl_2^{2-}$ this motion occurs at a lower temperature than for $GaCl_2^{2-}$. If an extrapolation is again permitted, then the primary Tl^0 center should possess a similar reorientation motion even at liquid-helium temperatures. That this may be so is supported by the observation[24] that no optical anisotropy can be produced by polarized light in the primary Tl^0 absorption bands at 4.2 K.

A motion at such low temperatures should be some kind of a phonon-assisted tunneling motion. If this reorientation is sufficiently fast it can lead to several effects making the ESR observation of the primary Tl^0 very difficult. First, a sufficiently rapid bond switching between the three $\langle 100 \rangle$ directions will lead in ESR to a $TlCl_6^{6-}$ species rather than a $TlCl_2^{2-}$, and the former is estimated to have rather broad unresolved lines rather than the nicely resolved seven line shf structure for the latter. Second, rapid motions will tend to displace and broaden the ESR lines because motional averaging towards isotropic lines is expected to occur. Considering the size of both the g anisotropy and the Tl^0 hf interaction, very high reorientation rates ($\sim 10^{10}$ Hz) are required for complete averaging. Finally, very rapid reorientation will induce a fast electron spin relaxation also broadening the ESR lines. All the foregoing mechanisms may well explain why the ESR spectrum of the primary Tl^0 center has so far not been observed at X-band frequencies. The solution of this matter will, however, require further study.

The data on $Ga^0(1)$, $In^0(1)$, and $Ga^0(2)$, $In^0(2)$ obtained in this paper nicely confirm the conclusions obtained in Ref. 6 on the $Tl^0(1)$ and $Tl^0(2)$ defects. It appears that the models for the $M^0(1)$ and $M^0(2)$ heavy metal ion centers as presented in Figs. 8(b) and 8(c) are firmly established. Furthermore, the importance in the defect formation of the mobility of the negative ion vacancy above 220 K (in KCl) is again emphasized. Because spin-orbit and relativistic effects are smaller in Ga^0 and In^0 than in Tl^0 it was

possible to perform a simple analysis of the g and hf components. The hf analysis in particular has yielded a phenomenological insight into the behavior of the isotropic part of the Ga^0 and In^0 hf interaction under the influence of even and odd crystal fields. This hf behavior will be more fully discussed in a subsequent paper where the results of a relativistic many-body calculation of the hf interaction will be presented.[18]

Of the two remaining defects In^0 (ortho) and Ga^0 (axial) the latter one appears to have some interesting properties. The experimentally observed g values exhibit an "inverted" relationship, i.e., $\Delta g_\perp < \Delta g_\parallel$ which is rather anomalous when compared to the other Ga^0 centers, or to the In^0 and Tl^0 defects for that matter. Such a relationship could only be understood by accepting that Ga^0 (axial) is basically an orthorhombic center which exhibits a rapid reorientation motion between two equivalent Jahn-Teller distortions confined to a {100} plane. The existence of this motion made it possible to narrow down the most likely Ga^0 (axial) defect structures to the two presented in Figs. 9(b) and 9(c). In contrast, the absence of observable motions for In^0 (ortho) results in a greater number of possible defect structures, and it was not possible to narrow down that number.

In proposing structures for Ga^0 (axial) and In^0 (ortho) only positive and negative ion vacancies were considered as perturbing entities, and not, e.g., unintentional impurities (most likely Na^+, Br^-, or O_2^- in KCl) or radiation produced halogen interstitials. There is as yet no compelling need to use them and in fact in most, if not all, cases one can argue against the likelihood of them being present in the defect structure. Interstitial halogen ions trapped in the neighborhood of the heavy metal defect will most likely result in low-symmetry defect structures whose axes are tipped with respect to the crystal axes.[25] As for unintentional impurities we observe that one would have to accept a large preferential association of the M^+ dopant with the unintentional impurity, even at the relatively low M^+ doping levels we are using.

Finally we would like to mention that we have not observed $H(M^+)$-type defects, i.e., interstitial halogen atoms stabilized by substitutional $M^+(ns^2)$ impurities similar to the $H_A(Na^+)$ and $H_A(Li^+)$ centers in KCl. This is in contrast to $KCl:Pb^{2+}(6s^2)$ and $KCl:Sn^{2+}(5s^2)$ where $H_D(Pb^{2+})$ and $H_D(Sn^{2+})$-type defects have been observed.[26] Maybe the presence of a charge compensating cation vacancy for the latter ions makes a difference. It is also possible that the $H(M^+)$ ESR spectra are obscured by the presence of the strong M^0 spectra.

ACKNOWLEDGMENTS

[1]C. J. Delbecq, R. Hartford, D. Schoemaker, and P. H. Yuster, Phys. Rev. B 13, 3631 (1976).

[2]W. Frey and H. Seidel, Phys. Status Solidi B 66, K39 (1974).

[3]F. Van Steen and D. Schoemaker, Phys. Rev. B 19, 55 (1979).

[4]E. Goovaerts, A. Lagendijk, and D. Schoemaker, in Proceedings of the International Conference on Defects in Insulating Crystals, Gatlinburg, 1977 (unpublished), p. 153.

[5]E. Goovaerts, S. V. Nistor, I. Ursu, and D. Schoemaker, in Joint Ismar-Ampère Conference on Magnetic Resonance, Delft, 1980 (unpublished), p. 39.

[6]E. Goovaerts, J. Andriessen, S. V. Nistor, and D. Schoemaker, Phys. Rev. B 24, 29 (1981).

[7]C. J. Delbecq, A. K. Ghosh, and P. H. Yuster, Phys. Rev. 151, 699 (1966); 154, 797 (1967).

[8]I. Jaek and M. Kink, Phys. Status Solidi B 56, 375 (1973).

[9]C. J. Delbecq, Y. Toyozawa, and P. H. Yuster, Phys. Rev. B 9, 4497 (1974).

[10]W. Van Puymbroeck, J. Andriessen, and D. Schoemaker, in Proceedings of the 1980 Conference of the Condensed Matter Division of the European Physical Society, Antwerp, 1980 (unpublished), p. 69.

[11]Le Si Dang, R. Romestain, Y. Merle d'Aubigné, and A. Fukuda, Phys. Rev. Lett. 38, 1539 (1977); Le Si Dang, Y. Merle d'Aubigné, R. Romestain, and A. Fukuda, Solid State Commun. 26, 413 (1978).

[12]A mnemonic aid given in Ref. 6 is the following: The number X given between brackets in the $M^0(X)$ or $M^+(X)$ defect gives the number of the negative ion vacancies involved in the defect structure.

[13]J. P. Stott and J. H. Crawford, Phys. Rev. B 4, 630 (1971).

[14]From atomic data [Landolt-Börnstein, Atomen und Ionen (Springer-Verlag, Berlin, 1950)].

[15]J. H. Ammeter and D. C. Schlosnagle, J. Chem. Phys. 59, 4784 (1973).

[16]A. Altenberger-Siczek, Phys. Rev. B 15, 64 (1977).

[17]D. Schoemaker, Phys. Rev. B 7, 786 (1973).

[18]W. Van Puymbroeck, J. Andriessen, and D. Schoemaker Phys. Rev. B (in press).

[19]D. Schoemaker and E. L. Yasaitis, Phys. Rev. B 5, 4970 (1972).

[20]T. O. Woodruff and W. Känzig, J. Phys. Chem. Solids 5, 268 (1958).

[21]F. Lüty, in *Physics of Color Centers,* edited by W. B. Fowler (Academic, New York, 1968), p. 181.

[22]See P. G. Baranov and V. A. Khramtsov, Phys. Status Solidi B 101, 153 (1980), and references therein.

[23]D. Schoemaker (unpublished results).

[24]C. J. Delbecq and P. H. Yuster (private communication).

[25]See, e.g., D. Schoemaker and A. Lagendijk, Phys. Rev. B 15, 115 (1977), and references therein.

[26]W. Van Puymbroeck and D. Schoemaker, Phys. Rev. B 23, 1670 (1981).